RSC Advances

PAPER

View Article Online
View Journal | View Issue

Open Access Article. Published on 03 January 2025. Downloaded on 10/27/2025 12:00:44 PM.
This article is licensed under a Creative Commons Attribution-NonCommercial 3.0 Unported Licence.

Check for updates

Cite this: *RSC Adv.*, 2025, **15**, 398

Imidazolium-based ionic liquid functionalized chiral metal–organic framework as an efficient catalyst for asymmetric catalytic sulfoxidation†

Shiye Li,[ab] Yudan Chai[b] and Jian Zhang *[b]

Ionic liquid (IL) units in heterogeneous catalysts exhibit synergistic effects to enhance catalytic performance and stabilize catalytically active centers, while also preventing the degradation of catalysts during the reaction process. Ionic liquid units in IL-functionalized CMOF catalysts enhance their catalytic performance in a synergistic manner. However, not only are the yields of IL-functionalized CMOFs obtained with post-synthesis methods low, but they also lead to blocking of the MOF pores and leaching of the ionic liquid. Hence, we designed and synthesized IL-functionalized chiral Ti(salen)-derivatized dicarboxylic acid as a linker coordinated with zinc nitrate to form ionic liquid functionalized CMOF **(IL-Ti(salen) CMOF-*n*)** (*n* = 1 and 2) catalysts. The synthesised **IL-Ti(salen) CMOF-*n*** catalyst was characterized by FT-IR, PXRD, SEM, TEM, TGA and N_2 adsorption–desorption, and the catalytic performance of the **IL-Ti(salen) CMOF-*n*** was assessed using the asymmetric oxidation of methyl phenyl sulfide as a model reaction and H_2O_2 as an oxidant. (*R*)-Methyl phenyl sulfoxide with remarkable chemoselectivity (93%) and enantioselectivity (>99%) was obtained under the optimal reaction conditions. Furthermore, the catalysts demonstrated excellent recyclability after seven consecutive reuses without obvious loss of activity. This work highlights the significance of developing a new type of ionic liquid functionalized chiral heterogeneous catalyst with remarkable catalytic performance, and provides valuable guidance for the design and preparation of novel catalysts for asymmetric catalysis.

Received 17th October 2024
Accepted 18th December 2024

DOI: 10.1039/d4ra07458k

rsc.li/rsc-advances

1. Introduction

Ionic liquids (ILs), consisting of organic cations and inorganic anions, are a type of molten salt that remain in liquid form at room temperature.[1] ILs have many exceptional properties, such as nonvolatility, low vapor pressure, strong dissolution, high thermal stability, inherent structure tunability and good catalytic activity.[2–5] As a result of these unique properties, ILs have increasingly become a focus of attention in catalysis, functional material synthesis, batteries, and adsorption separation.[6–9] Especially in catalysis, ILs act as complex solvents, capable of dissolving both organic and inorganic compounds during the reaction, thereby promoting the interaction between the substrate and the solvent and changing the reaction rate and selectivity. For example, not only does the use of ILs as solvents for the CO_2 cycloaddition reaction result in CO_2 and epoxides being dissolved, but also the nature and concentration of cations and anions in the ILs facilitates ring-opening of the epoxides, thus increasing both conversion rates and selectivity.[10,11] Using ILs as solvents, Ru-based catalysts have been synthesized to catalyze acetylene (C_2H_2) hydrochlorination.[12] It is demonstrated that ILs can stabilize Ru-based catalysts and create an ionic liquid based nano-environment on the surface of the catalyst to enhance its interaction with substrates, providing a homogeneous solvent environment and facilitating mass transfer. However, the widespread use of ILs has been severely hindered by operational difficulties due to their high synthesis costs, high characteristic viscosity, and low diffusion coefficient, as well as the nature of homogeneous catalysts, which are difficult to separate and recover.[13–15] To circumvent this problem, more rational strategies have been developed such as the immobilisation of ionic liquids onto silica materials, polymers, and biopolymers, which is widely regarded as an effective strategy.[16–19] For example, an ionic liquid is loaded on a $PdCl_2$–$Cu_3(BTC)_2$ MOF material to form a $PdCl_2$-ILs/$Cu_3(BTC)_2$ catalyst for the selective oxidation of cyclohexene, using molecular oxygen as the oxidant.[20] It was found that the catalytic activity of $PdCl_2$-ILs/$Cu_3(BTC)_2$ was superior to that of $PdCl_2$/$Cu_3(BTC)_2$ in terms of reaction rate and TOF value, which could be attributed to the fact that the ILs favored the homogeneous dispersion of $PdCl_2$ in the interior of the MOF. ILs of different amounts were anchored to the skeleton of iron-porphyrinic Zr-MOFs to form IL_x@MOF-526, which catalyzed the photochemical reduction of

[a]School of Chemical Engineering, Shanxi Institute of Science and Technology, No. 666, Lingqin Line, Jincheng, 048000, China

[b]School of Chemistry and Chemical Engineering, Shanxi University, Taiyuan, 030006, China. E-mail: zhangjian@sxu.edu.cn

† Electronic supplementary information (ESI) available. See DOI: https://doi.org/10.1039/d4ra07458k

© 2025 The Author(s). Published by the Royal Society of Chemistry

Open Access Article. Published on 03 January 2025. Downloaded on 10/27/2025 12:00:44 PM. This article is licensed under a Creative Commons Attribution-NonCommercial 3.0 Unported Licence.

CO_2.[5] The results indicated that the microenvironments of the IL_x@MOF-526 were modulated upon the introduction of the ILs, which enhanced CO_2 adsorption and charge transfer, thus improving the efficiency and selectivity of CO_2 photoreduction compared to the parent Zr-MOFs. Imidazolium ionic liquids were immobilized on DhaTat-COF carriers to form DhaTat-COF-IL *via* covalent grafting, which subsequently catalyzed a cycloaddition reaction to produce cyclic carbonates.[21] This finding indicates that the DhaTat-COF-IL demonstrated excellent catalytic performance compared to an IL with equal numbers of active sites, attributed to the synergistic effect between the IL and DhaTat-COF in catalyzing cycloaddition reactions. However, their widespread application is somewhat restricted by low loading of catalytic sites, poor hydrothermal stability, and susceptibility to corrosion in acidic or alkaline environments.

Metal–organic frameworks (MOFs), which consist of metal ions/clusters and organic linkers, are porous and versatile crystalline materials due to their large surface areas, high porosity, tunable pore size and functionalities, with potential applications in gas adsorption, batteries, sensors, drug delivery, purification, and effective heterogeneous catalysis.[22–27] In particular, chiral MOFs (CMOFs) are ideally suited for heterogeneous asymmetric catalysis because they have excellent structural intelligibility, tunable confined space, large surface areas and versatile chiral functionalization.[28] Furthermore, CMOFs with chiral confined nanospaces are able to further modulate the chiral environment around the active sites and can often provide additional strong multidirectional interactions between the substrates and the chiral environment of the cavities. More importantly, an imidazolium-based IL modified chiral nanospace can not only significantly promote the catalytic performance, but also stabilize the catalytically active center.[29] On the basis of these significant benefits, researchers have focused on the incorporation of ionic liquids onto CMOFs and the construction of multifunctional heterogeneous catalysts. Generally, there are two methods for immobilizing ionic liquids onto MOFs, namely ionothermal synthesis and post-synthesis modification methods.[17] Unfortunately, the cations and anions of the IL seriously affect the structure of the MOF in the ionothermal synthesis method.[30] Similarly, the post-synthesis not only results in low yields but also leads to potential issues such as blocking of the MOF pores and leaching of the ionic liquid.[31,32] Hence, the synthesis of the desired CMOFs using premodified ligands is a reasonable approach to solve this problem.

Chiral sulfoxides are important synthetic intermediates for the construction of various chiral drugs and biologically active compounds.[33,34] The asymmetric oxidation of sulfides is an attractive and important method to obtain chiral sulfoxides.[35] Meanwhile, the oxidation of sulfides with H_2O_2 as the oxidant is a green and efficient method for the preparation of sulfoxides, as H_2O_2 is widely regarded as a green and effective oxidant in organic oxidations.[36] Hence, we designed and synthesized a family of ionic liquid functionalized chiral MOFs (**IL-Ti(salen) CMOF-*n***) coordinated to zinc nitrate *via* ionic liquid-functionalized ligands, and used them for the asymmetric oxidation of sulfides. Compared with the postsynthetic method, the IL-functionalized ligand yield is high and the resulting CMOF material thereby exhibits a high density of IL active sites within its nanospaces, which will promote the catalytic performance of the **IL-Ti(salen) CMOF-*n*** catalyst in a cooperative manner. To further verify the synergistic effect of ionic liquids, we then synthesized chiral MOFs (**Ti(salen) CMOF**) without ionic liquid modification using Ti(salen)-derived dicarboxylic acid ligands coordinated to zinc nitrate. As presented in this study, the **IL-Ti(salen) CMOF-*n*** catalyst demonstrated excellent catalytic activity and enantioselectivity in the asymmetric oxidation of sulfides. Furthermore, the ionic liquid functionalized chiral MOF could be readily recycled and reused repeatedly at least seven times without obvious reduction of its catalytic performance, which may open a new window for the synthesis of ionic liquid functional materials in the practice of chiral drug synthesis in an environmentally friendly manner.

2. Experimental

2.1 Chemicals and materials

Methyl phenyl sulfide, ethyl phenyl sulfide, *n*-butyl phenyl sulfide, 4-methylphenyl methyl sulfide, 2-methoxyphenyl methyl sulfide, 4-methoxyphenyl methyl sulfide, 2-chlorophenyl methyl sulfide, 3-chlorophenyl methyl sulfide, 3-bromophenyl methyl sulfide, 4-*n*itrophenyl methyl sulfide, 4-bromophenyl methyl sulfide, phenyl vinyl sulfide, and benzyl methyl sulfide were purchased from Macklin. Proline, 1*H*-imidazole-1-carboxylate, 2-methyl-1*H*-imidazole-1-carboxylate, $Zn(NO_3)_2 \cdot 6H_2O$, paraformaldehyde, and 3-(*tert*-butyl)-5-(chloromethyl)-2-hydroxybenzaldehyde were bought from J&K. Other commercially available chemicals were obtained from local suppliers.

2.2 Characterization

Fourier transfer infrared (FT-IR) spectra were analysed with a resolution of 4 cm^{-1} in the range of 450–4000 cm^{-1} using a NEXUS spectrometer. Transmission electron microscopy (TEM) micrographs were obtained on a JEM-2100 instrument at an accelerating voltage of 200 kV. Scanning electron microscopy (SEM) was performed with a Nova NanoSEM 230 apparatus operating at an accelerating voltage of 15 kV. Thermogravimetric (TGA) analysis was carried out using a Netzch STA409PC instrument. Nitrogen adsorption–desorption measurements were performed on a TriStar 3000-Micromeritics instrument. Powder X-ray diffraction (PXRD) patterns were obtained using a 2550 diffractometer (Rigaku Corporation) equipped with a copper X-ray source and a scintillation counter detector. Contents of zinc and titanium in the samples were determined by inductively coupled optical emission spectra (ICP-OES) on an Agilent 5110. Nuclear magnetic resonance (NMR) spectra were recorded using a BRUKER AVANCE-500 spectrometer. The product chemoselectivity for asymmetric oxidation was determined by using a GC-2010plus equipped with a DB-17 (30 m × 0.32 mm × 0.50 μm) column. The ee was determined using an HPLC system (Hitachi L-20AT) with a Daicel Chiralpak AD column.

Open Access Article. Published on 03 January 2025. Downloaded on 10/27/2025 12:00:44 PM.
This article is licensed under a Creative Commons Attribution-NonCommercial 3.0 Unported Licence.

2.3 Synthesis of ionic liquid-functionalized chiral MOF and Ti(salen) CMOF

2.3.1 Synthesis of IL-Ti(salen) CMOF-*n* (*n* = 1 and 2). The ionic liquid-functionalized chiral MOF **IL-Ti(salen) CMOF-*n*** was prepared by a solvothermal method, as shown in Scheme 1.[37,38] A mixture of $Zn(NO_3)_2 \cdot 6H_2O$ (0.67 mmol), different IL-Ti(salen)-derived dicarboxylic bridging linkers (0.24 mmol), and DMF (120 mL) in a capped vial were heated at 80 °C for 72 h. After cooling to room temperature, faint yellow powders were obtained. The powders were collected *via* centrifugation, washed with *N*,*N*-dimethylformamide and hexane, and dried under vacuum at 60 °C for 12 h, affording the ionic liquid-functionalized chiral MOF **IL-Ti(salen) CMOF-*n* (*n* = 1 and 2)**. For the typical **IL-Ti(salen) CMOF-1**: FT-IR (KBr): γ_{max} cm^{-1} 3431, 2964, 2858, 1650, 1443, 1389, 1322, 1200, 1120, 1019, 815, 782, 692, 637, 551. Zinc content: 0.80 mmol g^{-1}, titanium content: 1.28 mmol g^{-1}.

2.3.2 Synthesis of Ti(salen) CMOF. To investigate the synergistic effect of the ionic liquid, **Ti(salen) CMOF** was prepared as a control catalyst, as shown in Scheme 2.[39] A mixture of $Zn(NO_3)_2 \cdot 6H_2O$ (0.67 mmol), Ti(salen)-derived dicarboxylic linkers (0.24 mmol), and DMF (120 mL) in a capped vial were heated at 80 °C for 72 h. After cooling to room temperature, brown powders were obtained. The powders were collected *via* centrifugation, washed with *N*,*N*-dimethylformamide and hexane, and dried under vacuum at 80 °C for 12 h, affording the chiral MOF **Ti(salen) CMOF**. For the **Ti(salen) CMOF**: FT-IR (KBr): γ_{max} cm^{-1} 3418, 2964, 2858, 1650, 1439, 1371, 1303, 1209, 1142, 1088, 872, 791, 637, 551. Zinc content: 0.93 mmol g^{-1}, titanium content: 1.07 mmol g^{-1}.

2.4 Asymmetric sulfoxidation over IL-Ti(salen) CMOF in methanol

The selected catalyst was stirred with sulfides (0.5 mmol) in methanol (2.0 mL) at 25 °C. H_2O_2 (30 wt%, 0.6 mmol) was then added dropwise over 15 min. The resulting mixture was stirred at 25 °C. The reaction progress was monitored by TLC. After the reaction, the catalyst was separated from the reaction system through high speed centrifugation (10 000 rpm). The recovered catalyst was washed with methanol, dried in a vacuum, and finally recharged with fresh substrate for the next catalytic cycle. The organic layers were quantitatively analyzed by a GC-2010plus equipped with a DB-17 (30 m × 0.32 mm × 0.50 μm) column and an FID detector. Further purification of the residue by chromatography on silica gel afforded the condensation products as a white solid. The pure chiral sulfoxides were identified by ^1H and ^{13}C NMR spectroscopy. Ee values of the products were determined by HPLC analysis using Daicel Chiralpak AD columns. Detailed NMR and HPLC analyses for the sulfoxides are available in the ESI.†

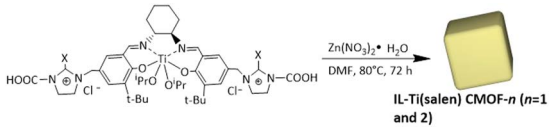

Scheme 1 The synthesis of IL-Ti(salen) CMOF-*n* (*n* = 1 and 2).

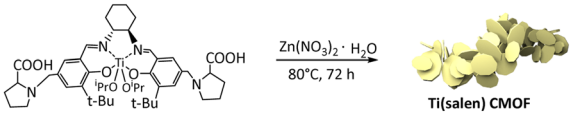

Scheme 2 The synthesis of Ti(salen) CMOF.

3. Results

3.1 Preparation of catalysts

Chiral MOFs (CMOFs) are best suited for heterogeneous asymmetric catalytic oxidation because of their excellent structural intelligibility, tunable confined space, large surface areas and versatile chiral functionalization.[40] In particular, the chiral nanospace of IL-functionalized CMOFs not only significantly improves the catalytic performance, but also stabilizes the catalytically active center.[29] However, the synthesis of IL-functionalized CMOFs using ionothermal synthesis and post-synthesis modification methods has low yields, leading to the blocking of the MOF pores and leaching of the ionic liquid.[31] To address these issues, we used IL-functionalized chiral Ti(salen)-derived dicarboxylic acids as linkers to construct CMOF catalysts. This strategy improves the yield of IL-functionalized chiral MOFs, and the resulting CMOF material exhibits a high density of ionic liquid active sites in its nanospace, which would contribute to improving the catalytic performance of the **IL-Ti(salen) CMOF-*n*** catalysts in a cooperative manner. Moreover, in order to further understand the synergistic effect of ionic liquids, we synthesized the chiral MOF (**Ti(salen) CMOF**) without ionic liquid modification as a comparative catalyst. Finally, the catalytic performance of the above chiral heterogeneous catalyst is investigated for the asymmetric oxidation of sulfides. The structure of the acquired catalyst is characterized by FT-IR, PXRD, SEM, TEM, N_2 adsorption–desorption and TGA measurements.

3.2 Characterization of catalysts

3.2.1 FT-IR, PXRD and TGA. The coordination of ionic liquid-functionalized chiral Ti(salen) derived dicarboxylic

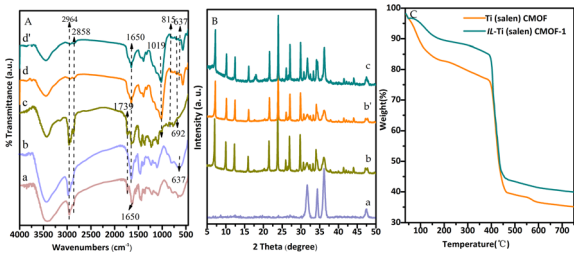

Fig. 1 FT-IR spectra of the Ti(salen)-derived dicarboxylic bridging linker (A-a), **Ti(salen) CMOF** (A-b), IL-Ti(salen)-derived dicarboxylic bridging linker (L_1) (A-c), the fresh **IL-Ti(salen) CMOF-1** (A-d) and the reused **IL-Ti(salen) CMOF-1** (A-d′); PXRD patterns of **Ti(salen) CMOF** (B-a), **IL-Ti(salen) CMOF-1** (B-b), the reused **IL-Ti(salen) CMOF-1** (B-b′) and **IL-Ti(salen) CMOF-2** (B-c); TGA (C) analysis of **Ti(salen) CMOF** and **IL-Ti(salen) CMOF-1**.

 © 2025 The Author(s). Published by the Royal Society of Chemistry

Open Access Article. Published on 03 January 2025. Downloaded on 10/27/2025 12:00:44 PM.
This article is licensed under a Creative Commons Attribution-NonCommercial 3.0 Unported Licence.

linkers with zinc(II) ions in **IL-Ti(salen) CMOF-*n* (*n* = 1 and 2)** was confirmed by FT-IR, with **Ti(salen) CMOF** as a comparative catalyst. **IL-Ti(salen) CMOF-1** was chosen as a typical catalyst for the structural identification. Fig. 1 shows the FT-IR spectra of typical **IL-Ti(salen) CMOF-1**, with **Ti(salen) CMOF** as well as IL-Ti(salen)-1 derived dicarboxylic acids for comparison. Clearly, the IL-Ti(salen)-1 derived dicarboxylic acids showed two characteristic bands at 1739 and 1650 cm^{-1}, corresponding to the skeletal vibrations of the carboxyl functional and imine groups (Fig. 1c).[41,42] Meanwhile, the characteristic band shifts to 1650 cm^{-1} and overlaps with the characteristic absorption peak of the imine groups when the IL-salen ($n = 1$) derived dicarboxylic acids are treated with zinc nitrate hexahydrate (Fig. 1d).[43] The significant red shift provides convincing evidence that the carboxylic acid group of the IL-Ti(salen)-1 derived dicarboxylic acids interacted with the zinc(II) ion during the solvothermal synthesis.[44] Interestingly, a new strong band associated with the stretching vibrations of the Zn–O–C group was observed at 637 cm^{-1} in the FT-IR spectrum of **IL-Ti(salen) CMOF-1** and **Ti(salen) CMOF** (Fig. 1d and b).[45] Additional characteristic bands at 2942 and 2864 cm^{-1} associated with the methylene in the 1, 2-aminocyclohexane motif further confirmed the presence of the IL-Ti(salen) moiety in the CMOF framework (Fig. 1d).[42,46] Compared to **IL-Ti(salen) CMOF-1**, **Ti(salen) CMOF** showed the absence of the characteristic stretching vibration of the imidazole ring at 1019, 815 and 692 cm^{-1} in the FT-IR (Fig. 1b *vs.* d). It can be seen that the chiral cavity modified by ionic liquid functionalization IL-Ti(salen) derived dicarboxylic linkers renders all active centres accessible to the substrate, which enhanced the catalytic efficiency of the chiral MOF in asymmetric sulfoxidation.

The crystallinity of **Ti(salen) CMOF** and **IL-Ti(salen) CMOF-*n* (*n* = 1 and 2)** were investigated using PXRD patterns, as shown in Fig. 1B. The pattern for **Ti(salen) CMOF** has three broad peaks at 31.7, 34.4, and 36.2, which indicates the nature of the two-dimensional structure of **Ti(salen) CMOF** (Fig. 1B-a). A similar observation of XRD patterns has been previously reported for 2D MOF nanosheets.[47] The phase purity of **IL-Ti(salen) CMOF-*n* (*n* = 1 and 2)** indicated high crystallinity and different diffraction patterns were exhibited compared to the **Ti(salen) CMOF** (Fig. 1B-b, c *vs.* a). Furthermore, PXRD patterns also suggested that the crystal structures were identical for **IL-Ti(salen) CMOF-1** and **IL-Ti(salen) CMOF-2** (Fig. 1B-b and c).

TGA was performed to assess the thermal stability of the synthesized **Ti(salen) CMOF** and representative **IL-Ti(salen) CMOF-1** materials, as shown in Fig. 1C. The first step indicated a weight loss stage from 35 °C to 200 °C, which was attributed to the evaporation of adsorbed and coordinated water and the organic solvent inside or outside the pores of the **Ti(salen) CMOF** and **IL-Ti(salen) CMOF-1** frameworks. The **Ti(salen) CMOF** and **IL-Ti(salen) CMOF-1** underwent a second weight loss from 200 °C to 480 °C, which was mainly put down to the partial decomposition of functional groups of **Ti(salen) CMOF** and **IL-Ti(salen) CMOF-1** backbones. The **Ti(salen) CMOF** and **IL-Ti(salen) CMOF-1** underwent the final weight loss step above 480 °C due to the collapse of their backbones and decomposition into metal oxides. Interestingly, the thermal stability of **IL-Ti(salen) CMOF-1** was found to be better than that of **Ti(salen) CMOF**, which was attributed to the fact that the introduction of imidazolium-based ionic liquids into the ligand of **IL-Ti(salen) CMOF-1** significantly improved its stability. These results indicated that the stability of the CMOF synthesized from the ionic liquid-modified linker was significantly higher than that of the **Ti(salen) CMOF** catalyst. This finding indicates that the pore-confined catalyst modified by ionic liquid possesses excellent thermal stability.

3.2.2 SEM and TEM. SEM and TEM images provide direct information on the morphology of **Ti(salen) CMOF** and **IL-Ti(salen) CMOF-*n* (*n* = 1 and 2)**, as shown in Fig. 2. It is clear that **Ti(salen) CMOF** exhibits a flake morphology structure in the SEM image (Fig. 2A). However, the morphology of **IL-Ti(salen) CMOF-*n* (*n* = 1 and 2)** synthesized from ionic liquid-modified ligands was different from that of **Ti(salen) CMOF**, exhibiting the formation of a block-shaped morphology with a range of sizes in the micrometer range (Fig. 2B and D). Meanwhile, the TEM image also showed cubes of typical **IL-Ti(salen) CMOF-1**, consistent with the SEM image (Fig. 2F). Furthermore, the TEM image of **Ti(salen) CMOF** exhibited a crystalline sheet structure, further proving that the morphology of CMOF synthesized from ligands without ionic liquid modification was different from that of **IL-Ti(salen) CMOF-1** (Fig. 2E).

3.2.3 Nitrogen adsorption–desorption. In order to identify the BET surface and porosity of the **Ti(salen) CMOF** and the **IL-Ti(salen) CMOF-*n* (*n* = 1 and 2)** samples, N_2 adsorption–desorption analyses were performed as shown in Fig. 3. Typical type-IV adsorption behaviours were observed for the **Ti(salen) CMOF** and **IL-Ti(salen) CMOF-*n* (*n* = 1 and 2)**, indicating that they are typical mesoporous materials (Fig. 3 A–C).[48,49] Meanwhile, **IL-Ti(salen) CMOF-1** and **IL-Ti(salen) CMOF-2** showed H4-type hysteresis loops in the pressure range of $P/P_0 = 0.5$–1.0, further suggesting that this type of material has certain mesoporous properties (Fig. 3B and C). Based on the N_2 adsorption isotherms, the BET surface area was calculated to be 63.6 $m^2\ g^{-1}$

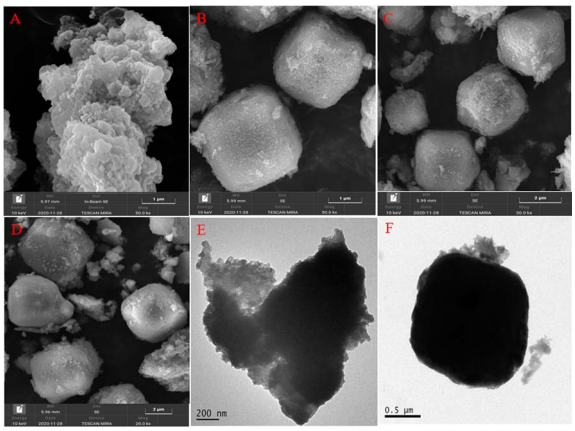

Fig. 2 SEM images of Ti(salen) CMOF (A), fresh IL-Ti(salen) CMOF-1 (B), reused IL-Ti(salen) CMOF-1 (C), IL-Ti(salen) CMOF-2 (D); TEM images of Ti(salen) CMOF (E) and IL-Ti(salen) CMOF-1 (F).

Open Access Article. Published on 03 January 2025. Downloaded on 10/27/2025 12:00:44 PM.
This article is licensed under a Creative Commons Attribution-NonCommercial 3.0 Unported Licence.

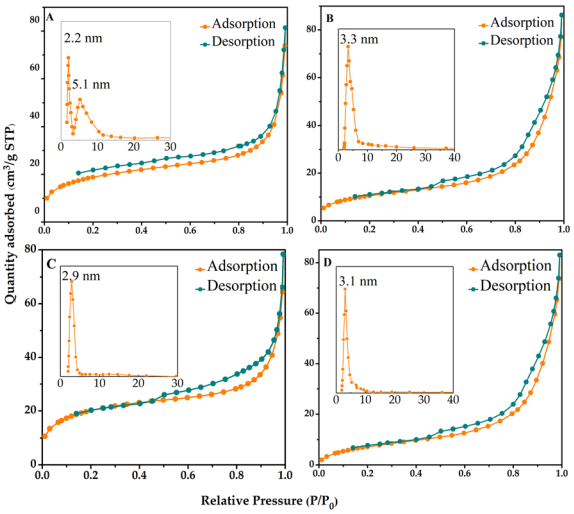

Fig. 3 Nitrogen adsorption–desorption of Ti(salen) CMOF (A), IL-Ti(salen) CMOF-1 (B), IL-Ti(salen) CMOF-2 (C) and reused IL-Ti(salen) CMOF-1 (D).

for **Ti(salen) CMOF** (Fig. 3A), whereas for the **IL-Ti(salen) CMOF-*n* (*n* = 1 and 2)**, the surface areas are even higher than those of **Ti(salen) CMOF** (Fig. 3B, C *vs.* A), 67.7 and 67.2 $m^2\ g^{-1}$, respectively. The pore size distribution curves of **IL-Ti(salen) CMOF-1** and **IL-Ti(salen) CMOF-2** are centered at 3.3 and 2.9 nm, which are larger than the 2.2 nm pore size of **Ti(salen) CMOF**. This huge increase of the accessible internal volume and open channel size in the **IL-Ti(salen) CMOF-1** and **IL-Ti(salen) CMOF-2** structures is crucial for enhanced asymmetric catalytic performance by facilitating the diffusion of reactants and products. However, the **Ti(salen) CMOF** nanosheets also exhibit a larger pore size of 5.1 nm, which may be due to the slit-like pores formed by aggregation of **Ti(salen) CMOF** nanosheets during the synthesis process.[50]

3.3 Catalytic performances

Benefiting from the incorporated chiral Ti(salen) moiety and imidazolium-based ionic liquid unit as well as large surface area and chiral cavities, the obtained **IL-Ti(salen) CMOF-*n* (*n* = 1 and 2)** are expected to be potential heterogeneous catalysts for asymmetric sulfoxidation. As shown in Table 1, the **IL-Ti(salen) CMOF-*n*** exhibited better catalytic activity and chemoselectivity in sulfide oxidation (Table 1, entries 1–2). In particular, **IL-Ti(salen) CMOF-1** is a highly effective catalyst for the asymmetric oxidation of methyl phenyl sulfide to (*R*)-methyl phenyl sulfoxide with remarkable chemoselectivity (93%) and enantioselectivity (>99%) (Table 1, entry 1). In contrast, the chemoselectivity (77%) and enantioselectivity (86%) were lower when neat Ti(salen) complex was used under identical conditions (Table 1, entry 4). It was found that the immobilization of the chiral Ti(salen) active site in the cavity of **IL-Ti(salen) CMOF-1** provided better chemoselectivity than the neat Ti(salen) complex by encapsulating substrates and concentrating reactants in the chiral confined cavity through host–guest interactions (Table 1, entry 1 *vs.* 4). More importantly, the framework-confined catalyst provided significantly higher chemoselectivity than the corresponding neat Ti(salen) complex, probably due to the steric restrictions imposed by the inner block of the confined network. Moreover, multiple zinc–benzoate complexes arranged on the framework of **IL-Ti(salen) CMOF-1** may enforce an intramolecular cooperative reaction pathway, resulting in enhanced reaction rates and higher chemoselectivity (Table 1, entry 5). Finally, it was found that the pore size of **IL-Ti(salen) CMOF-*n*** has an impact on substrate diffusion and product chemoselectivity. Apparently, the conversion of **IL-Ti(salen) CMOF-2** was only 75% compared to **IL-Ti(salen) CMOF-1**, presumably a result of the small pore size that cannot allow free diffusion of methyl phenyl sulfide and H_2O_2 reagents (Table 1, entry 2 *vs.* 1). Meanwhile, the chemoselectivity of the (*R*)-methyl phenyl sulfoxide product of the **IL-Ti(salen) CMOF-2** catalyst was also low, only 90%. By comparing the above results, we can speculate that the chiral MOF catalyst possesses suitable pore channels and pore size, can make the Ti(salen) active center on the framework more flexible to access the reactants, and can promote the reaction smoothly in methanol.[51]

Table 1 Results of the asymmetric oxidation of methyl phenyl sulfide under different catalysts[a]

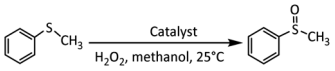

Entry	Catalyst	Conv.[b] (%)	Sel.[c] (%)	ee[d] (%)
1	**IL-Ti(salen) CMOF-1**	86	93	>99
2	**IL-Ti(salen) CMOF-2**	75	90	99
3	**Ti(salen) CMOF**	60	84	98
4	Ti(salen) complex	92	77	86
5	Zn-complex	33	>99	No

[a] Catalyst (6 mg), substrate (0.5 mmol), H_2O_2 (30 wt%, 0.6 mmol, added in 15 min), methanol (2.0 mL), 60 min, 25 °C. [b] Determined by GC. [c] Chemoselectivity to chiral sulfoxide (determined by GC). [d] Determined by HPLC (Daicel Chiralpak AD column).

In addition to the **IL-Ti(salen) CMOF-*n*** structure, the imidazolium-based IL fraction in the chiral cavity was also essential for the cooperative catalysis. Notably, the catalytic activity of **Ti(salen) CMOF** was much lower than that of **IL-Ti(salen) CMOF-*n*** under identical reaction conditions. Only 60% conversion of methyl phenyl sulfide with 84% chemoselectivity was obtained over the **Ti(salen) CMOF** (Table 1, entry 3). The results point to the necessity of the imidazolium-based IL moiety in the cooperative catalysis. More importantly, the imidazolium-based ionic liquid linker was a flexible linker that could allow conformational freedom of all Ti(salen) active sites in the MOF framework, thereby making the active site of the **IL-Ti(salen) MOF-*n*** catalyst more accessible to reagents.[52] Furthermore, the imidazolium-based IL moiety created an IL microenvironment on the CMOF framework, which rendered the catalytic sites more compatible, thereby tuning **IL-Ti(salen) CMOF-*n*** into an efficient catalyst for this reaction.[53]

3.3.1 Effect of the amount of IL-Ti(salen) CMOF-1 catalyst and reaction time. In order to determine the optimal conditions

 © 2025 The Author(s). Published by the Royal Society of Chemistry

Open Access Article. Published on 03 January 2025. Downloaded on 10/27/2025 12:00:44 PM.
This article is licensed under a Creative Commons Attribution-NonCommercial 3.0 Unported Licence.

for the asymmetric sulfoxidation reaction, key parameters such as the reaction time and catalyst amount were also explored. As shown in Fig. 4A, the conversion of methyl phenyl sulfide gradually increases from 16% to 86% when the reaction time is increased from 10 to 60 min. When the reaction time was extended to 70 min, the conversion of methyl phenyl sulfide exhibited no significant change, but the chemoselectivity and ee of the product were reduced to 90% and 98%. With the extension of time, the chemoselectivity and ee of the product began to decrease, possibly due to the decrease in the concentration of methyl phenyl sulfide and H_2O_2, and the inability to separate the product after the transformation of the reaction substrate. As shown in Fig. 4B, the amount of **IL-Ti(salen) CMOF-1** catalyst could significantly influence the oxidation of methyl phenyl sulfide. The conversion of methyl phenyl sulfide increased gradually with the increase of **IL-Ti(salen) CMOF-1** catalyst dosage. When the amount of **IL-Ti(salen) CMOF-1** catalyst was increased to 6 mg, both the conversion of methyl phenyl sulfide and the chemoselectivity of (*R*)-methyl phenyl sulfoxide were the highest, 86% and 93%, respectively. However, both conversion and chemoselectivity showed a decreasing trend when the catalyst dosage was further increased. This may be attributed to the fact that an excessive amount of catalyst will hinder the diffusion, block the active sites, and reduce the catalytic efficiency, thereby resulting in a corresponding decrease in the conversion.

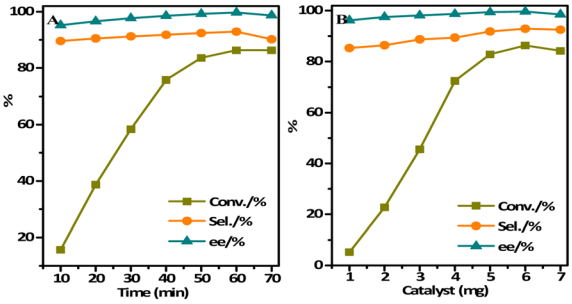

Fig. 4 Influences of reaction conditions on the catalytic activity for the asymmetric oxidation of methyl phenyl sulfide over IL-Ti(salen) CMOF-1: time (A) and catalyst dosage (B).

3.3.2 Substrate universality. To verify the synergistic effect and the enhanced activity, the catalytic performance of **IL-Ti(salen) CMOF-1** was investigated for the asymmetric oxidation of other arylalkyl sulfides, and the results are shown in Table 2. Notably moderate to good catalytic activity (40–85%) and high chemoselectivity (91–98%) for the catalyst **IL-Ti(salen) CMOF-1** were obtained with all the substrates, either electron-rich or electron-deficient (Table 2, entry 1–12), indicating high catalytic activity of the ionic liquid modified **IL-Ti(salen) CMOF-1**. However, low conversion was found when **IL-Ti(salen) CMOF-1** catalyzed the asymmetric oxidation of *n*-butyl phenyl sulfide, benzyl methyl sulfide and phenyl vinyl sulfide (Table 2, entries 2, 11 and 12). This may be due to the large size of *n*-butyl phenyl sulfide, benzyl methyl sulfide and phenyl vinylsulfide, which hindered diffusion and resulted in insufficient contact with the active site. Simultaneously, a sterically more demanding sulfide with a R_2 = 2-OCH_3 and benzyl phenyl were subjected to the reaction, and only 50% and 40% conversion were observed under identical reaction conditions (Table 2, entry 5 and 11). The above results indicate that the asymmetric sulfoxidation occurred mainly within the ionic liquid-modified confined cavities.[43] Nevertheless, the interesting point is that replacing the $-R_2$ group in PhSMe with a steric hindrance group, like 2-OCH_3 and benzyl phenyl, reduced conversion but increased enantioselectivity. This phenomenon has been attributed to the slower diffusion of the bulk substrate causing lower conversion, but the higher enantioselectivity may correspond to the increased geometrical constraints in the chiral confined cavities.[45] This positive confined catalysis with high activity and

Table 2 Results of asymmetric sulfoxidation in different arylalkyl sulfides[a]

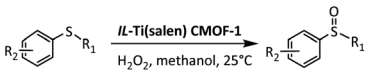

Entry	R_1	R_2	Catalyst	Conv.[b] (%)	Sel.[c] (%)	ee[d] (%)
1	C_2H_5	H	**IL-Ti(salen) CMOF-1**	85	91	99
2	C_4H_9	H		58	93	>99
3	CH_3	4-CH_3		80	98	96
4	CH_3	4-OCH_3		84	95	94
5	CH_3	2-OCH_3		50	97	99
6	CH_3	2-Cl		65	93	97
7	CH_3	3-Cl		70	95	95
8	CH_3	3-Br		68	94	97
9	CH_3	4-Br		71	91	99
10	CH_3	4-NO_2		65	92	90
11	CH_3	$-CH_2-Ph$		40	98	>99
12	$-CH{=}CH_2$	H		43	98	99

[a] Catalyst (6 mg), substrate (0.5 mmol), H_2O_2 (30 wt%, 0.6 mmol, added in 15 min), methanol (2.0 mL), 60 min, 25 °C. [b] Determined by GC. [c] Chemoselectivity to chiral sulfoxide (determined by GC). [d] Determined by HPLC (Daicel Chiralpak AD column).

Open Access Article. Published on 03 January 2025. Downloaded on 10/27/2025 12:00:44 PM.
This article is licensed under a Creative Commons Attribution-NonCommercial 3.0 Unported Licence.

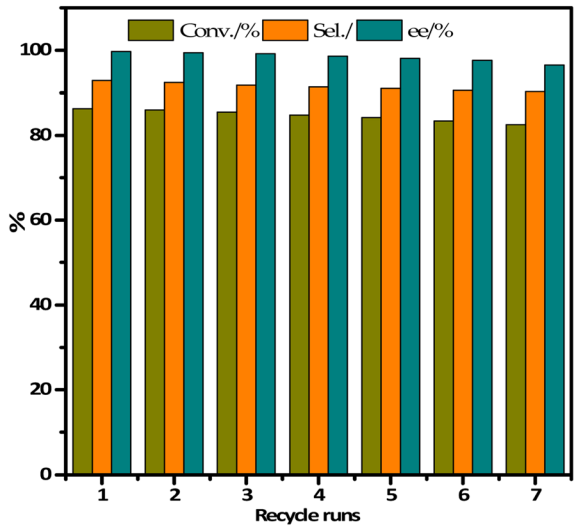

Fig. 5 Reusability of IL-Ti(salen) CMOF-1 in the asymmetric oxidation of methyl phenyl sulfide in methanol.

enantioselectivity provides further evidence that the asymmetric catalytic reaction might occur in the confined space of **IL-Ti(salen) CMOF-1**.

3.4 Reusability

In order to evaluate the stability of **IL-Ti(salen) CMOF-1** catalysts in the asymmetric oxidation of methyl phenyl sulfide, we investigated the recyclability of **IL-Ti(salen) CMOF-1** catalysts under optimal conditions. As shown in Fig. 5, after the **IL-Ti(salen) CMOF-1** catalyst had been reused seven times, the conversion of methyl phenyl sulfide and the chemical selectivity of the product exhibited no significant decrease. This indicates that **IL-Ti(salen) CMOF-1** exhibits excellent stability in the asymmetric oxidation of methyl phenyl sulfide. In addition, the recovered **IL-Ti(salen) CMOF-1** was further characterized by FT-IR, PXRD and N_2 adsorption–desorption. The FT-IR spectrum of the reused catalyst exhibited few differences compared to that of the freshly prepared sample (Fig. 1A-d *vs.* d′). Meanwhile, the PXRD pattern shows that the recovered catalyst is almost identical to the new catalyst (Fig. 1B-b *vs.* b′). In addition to this, the N_2 adsorption–desorption measurements also showed that the recovered samples had similar pore structure characteristics to the fresh catalysts (Fig. 3B *vs.* D), further indicating the good maintenance of the physicochemical properties of **IL-Ti(salen) CMOF-1** after the asymmetric catalysis. In summary, the **IL-Ti(salen) CMOF-1** catalyst possesses good stability and potential for the industrial application in asymmetric catalysis.

4. Conclusions

A series of ionic liquid functionalized chiral **IL-Ti(salen) CMOF-*n*** catalysts were successfully prepared by the coordination of ionic liquid functionalized chiral Ti(salen)-derived dicarboxylic acids with zinc nitrate. The obtained catalysts possessed large specific surface areas and a high density of ionic liquid active sites in their chiral confined cavities. Benefiting from the synergistic effect of the imidazolium-based ionic liquid unit and chiral confined nanospaces of the CMOFs, **IL-Ti(salen) CMOF-*n*** could efficiently catalyze the asymmetric oxidation of a sulfide with H_2O_2 as an oxidant. High chemoselectivity (up to 93%) and >99% ee for (*R*)-methyl phenyl sulfoxide were achieved over **IL-Ti(salen) CMOF-1** under ambient temperature conditions. Compared to **Ti(salen) CMOF**, the **IL-Ti(salen) CMOF-1** showed not only effective catalytic activity but also excellent recyclability, even after seven reuse cycles, by simple centrifugation without obvious loss of activity and stability. Moreover, the application of **IL-Ti(salen) CMOF-1** was further expanded to other arylalkyl sulfides, demonstrating efficient catalytic performance and high ee (up to 99%). This work provides valuable insights into the modulation of ionic liquid functionalized chiral catalytic centers in CMOFs, which can produce interesting synergistic effects and stabilize reaction intermediates, and systematically control the activity and selectivity of asymmetric catalysis.

Data availability

The data supporting this article have been included as part of the ESI.†

Author contributions

Jian Zhang conceived and designed the experiments. Shiye Li performed the experiments and analyzed the data. Yudan Chai helped perform the analysis with constructive discussions. The manuscript was written through contributions of all authors. All authors have given approval to the final version of the manuscript.

Conflicts of interest

There are no conflicts to declare.

Acknowledgements

The authors are grateful for the financial support provided by the 2023 annual Research Program (Free Exploration category) of Shanxi Province (202303021212302 and 202303021212303), the Natural Science Foundation of Shanxi Province (20210302123458), Higher Education Teaching Reform and Innovation Project of Shanxi Province (J20241914) and Scientific Research Foundation for Advanced Talents of Shanxi Institute of Science and Technology (2023005).

Notes and references

1 H. Weingärtner, *Angew. Chem., Int. Ed.*, 2008, **47**, 654–670.
2 M. D. Green and T. E. Long, *Polym. Rev.*, 2009, **49**, 291–314.
3 P. Sun and D. W. Armstrong, *Chim. Acta*, 2010, **661**, 1–16.
4 X. Kang, Q. Zhu, X. Sun, J. Hu, J. Zhang, Z. Liu and B. Han, *Chem. Sci.*, 2016, 7, 266–273.

 © 2025 The Author(s). Published by the Royal Society of Chemistry

Open Access Article. Published on 03 January 2025. Downloaded on 10/27/2025 12:00:44 PM.
This article is licensed under a Creative Commons Attribution-NonCommercial 3.0 Unported Licence.

5 X. Zhao, Q. Xu, J. Han, W. Zhang, H. Rao, D. Du, P. She and J. Qin, *ACS Appl. Mater. Interfaces*, 2024, **16**, 26272–26279.
6 J. P. Hallett and T. Welton, *Chem. Rev.*, 2011, **111**, 3508–3576.
7 M. Zeeshan, V. Nozari, S. Keskin and A. Uzun, *Chem. Res.*, 2019, **58**, 14124–14138.
8 Y. Meng, G. Wang, M. Xiao, C. Duan, C. Wang, F. Zhu and Y. Zhang, *J. Mater. Sci.*, 2017, **52**, 13192–13202.
9 A. Yohannes, J. Li and S. Yao, *J. Mol. Liq.*, 2020, **318**, 114304.
10 H. Jessica, Q. Diego, C. Gustavo, M. F. Oriol and I. Mauricio, *Catal. Lett.*, 2019, **149**, 1825–1832.
11 S. Gallardo-Fuentes, R. Contreras, M. Isaacs, J. Honores, D. Quezada, E. Landaeta and R. Ormazábal-Toledo, *J. CO_2 Util.*, 2016, **16**, 114–120.
12 Y. Li, Y. Dong, W. Li, Y. Han and J. Zhang, *Mol. Catal.*, 2017, **443**, 220–227.
13 A. Pourjavadi, S. H. Hosseini, M. Doulabi, S. M. Fakoorpoor and F. Seidi, *ACS Catal.*, 2012, **2**, 1259–1266.
14 M. Ding and H. Jiang, *ACS Catal.*, 2018, **8**, 3194–3201.
15 S. Sahoo, P. Kumar, F. Lefebvre and S. B. Halligudi, *Appl. Catal., A*, 2009, **354**, 17–25.
16 M. Garip and N. Gizli, *J. Mol. Liq.*, 2020, **310**, 113227.
17 X. Li, K. Chen, R. Guo and Z. Wei, *Chem. Rev.*, 2023, **123**, 10432–10467.
18 X. Zhang, T. Wang, Y. Wang, Y. Yan, S. Xue, S. Liu, Q. Ye, F. Zhou and W. Liu, *Chem. Eng. J.*, 2024, **493**, 152665.
19 K. R. Roshan, G. Mathai, J. Kim, J. Tharun, G. Park and D. Park, *Green Chem.*, 2012, **14**, 2933–2940.
20 Q. Luo, M. Ji, S. E. Park, C. Hao and Y. Li, *RSC Adv.*, 2016, **6**, 33048–33054.
21 Y. Ge, G. Cheng, Y. Zou and H. Ke, *J. Environ. Chem. Eng.*, 2024, **12**, 114417.
22 H. Daglar, H. C. Gulbalkan, G. Avci, G. O. Aksu, O. F. Altundal, C. Altintas, I. Erucar and S. Keskin, *Angew. Chem., Int. Ed.*, 2021, **60**, 7828–7837.
23 T. Chen, F. Wang, S. Cao, Y. Bai, S. Zheng, W. Li, S. Zhang, S. Hu and H. Pang, *Adv. Mater.*, 2022, **34**, 2201779.
24 Y. Jo, Y. K. Jo, J. Lee, H. W. Jang, I. Hwang and D. J. Yoo, *Adv. Mater.*, 2023, **35**, 2206842.
25 M. Wu and Y. Yang, *Adv. Mater.*, 2017, **29**, 1606134.
26 A. C. Kathalikkattil, R. Babu, R. K. Roshan, H. Lee, H. Kim, J. Tharun, E. Suresh and D. Park, *J. Mater. Chem. A*, 2015, **3**, 22636–22647.
27 S. Nandi, P. De Luna, T. D. Daff, J. Rother, M. Liu, W. Buchanan, A. I. Hawari, T. K. Woo and R. Vaidhyanathan, *Sci. Adv.*, 2015, **1**, e1500421.
28 K. Tanaka, K. Kubo, K. Iida, K. Otani, T. Murase, D. Yanamoto and M. Shiro, *Asian J. Org. Chem.*, 2013, **2**, 1055–1060.
29 J. Wang, Y. Tian, S. Zhang and Y. Zhang, *Appl. Catal., A*, 2022, **631**, 118477.
30 Z. Zhang, B. Liu, L. Xu and H. Jiao, *Dalton Trans.*, 2015, **44**, 17980–17989.
31 R. Dutta and A. Kumar, *J. Phys. D: Appl. Phys.*, 2017, **50**, 425302.
32 L. Ding, B. Yao, W. Jiang, J. Li, Q. Fu, Y. Li, Z. Liu, J. Ma and Y. Dong, *Inorg. Chem.*, 2017, **56**, 2337–2344.
33 L. Yang, B. Wang, X. Yin and Q. Zeng, *Chem. Rec.*, 2022, **22**, e202100242.
34 W. Wen, C. Yang, Z. Wu, D. Xiao and Q. Guo, *Adv. Sci.*, 2024, **14**, 2402429.
35 M. Zhang, Z. Tang, W. Fu, W. Wang, R. Tan and D. Yin, *Chem. Commun.*, 2019, **55**, 592–595.
36 M. Gao, R. Tan, P. Hao, Y. Zhang, J. Deng and D. Yin, *RSC Adv.*, 2017, **7**, 54570–54580.
37 W. Xi, Y. Liu, Q. Xia, Z. Li and Y. Cui, *Chem. Eur J.*, 2015, **21**, 12581–12585.
38 X. Guo, S. Qiu, X. Chen, Y. Gong and X. Sun, *Inorg. Chem.*, 2017, **56**, 12357–12361.
39 J. Chrzanowski, M. Rachwalski, A. M. Pieczonka, S. Leśniak, J. Drabowicz and P. Kiełbasiński, *Tetrahedron*, 2016, **72**, 2649–2655.
40 H. Zhang, L. Lou, K. Yu and S. Liu, *Small*, 2021, **17**, 2005686.
41 L. Li, X. Feng, X. Cui, Y. Ma, S. Ding and W. Wang, *J. Am. Chem. Soc.*, 2017, **139**, 6042–6045.
42 T. Liu, J. Liang, R. Xu, Y. Huang and R. Cao, *Chem. Commun.*, 2019, **55**, 4063–4066.
43 C. Xing, J. Deng, R. Tan, M. Gao, P. Hao and D. Yin, *Catal. Sci. Technol.*, 2017, **7**, 5944–5952.
44 Y. Shi, W. Zhang, B. F. Abrahams, P. Braunstein and J. Lang, *Angew. Chem., Int. Ed.*, 2019, **58**, 9453–9458.
45 Z. Yang, C. Zhu, Z. Li, Y. Liu, G. Liu and Y. Cui, *Chem. Commun.*, 2014, **50**, 8775–8778.
46 X. Zhang, W. Geng, C. Yue, W. Wu and L. Xiao, *J. Environ. Chem. Eng.*, 2016, **4**, 2565–2572.
47 G. Zhan, L. Fan, F. Zhao, Z. Huang, B. Chen, X. Yang and S. Zhou, *Adv. Funct. Mater.*, 2019, **29**, 1806720.
48 K. Deng, Z. Hou, X. Li, C. Li, Y. Zhang, X. Deng, Z. Cheng and J. Lin, *Sci. Rep.*, 2015, **5**, 7851.
49 L. Wu, G. Wan, N. Hu, Z. He, S. Shi, Y. Suo, K. Wang, X. Xu, Y. Tang and G. Wang, *Nanomaterials*, 2018, **8**, 451.
50 M. Zhao, Y. Wang, Q. Ma, Y. Huang, X. Zhang, J. Ping, Z. Zhang, Q. Lu, Y. Yu, H. Xu, Y. Zhao and H. Zhang, *Adv. Mater.*, 2015, **27**, 7372–7378.
51 M. B. Solomon, C. Hua, B. Chan, T. L. Church, S. M. Cohen, C. P. Kubiak, K. A. Jolliffe and D. M. D'Alessandro, *Dalton Trans.*, 2021, **50**, 12821–12825.
52 W. Wang, C. Li, Y. Pi, J. Wang, R. Tan and D. Yin, *Catal. Sci. Technol.*, 2019, **9**, 5626–5635.
53 Y. Zhang, R. Tan, M. Gao, P. Hao and D. Yin, *Green Chem.*, 2017, **19**, 1182–1193.